https://doi.org/10.5194/egusphere-2024-2971
Preprint. Discussion started: 9 October 2024

Long-term hazard of pyroclastic density currents at Vesuvius (Southern Italy) with maps of impact parameters

Pierfrancesco Dellino[1], Fabio Dioguardi[1], Roberto Sulpizio[1,2,3], Daniela Mele[1]

[1]Dipartimento di Scienze della Terra e Geoambientali, Università degli Studi di Bari "Aldo Moro", Bari, 70125, Italy
[2] Istituto Nazionale di Geofisica e Vulcanologia, Bologna section, Italy
[3] IGAG-CNR, Milano, Italy

Correspondence to: Pierfrancesco Dellino (pierfrancesco.dellino@uniba.it)

Abstract. The hazard of pyroclastic density currents (PDCs) at Vesuvius is investigated basing on past eruptions. Analysis is extended to all the eruptions that left substantial deposits on the ground.

The currents are bipartite, with a basal highly-concentrated part, which was fed from the impact of the eruptive fountain on the ground, and an overlying part generated by the squeezing of the collapsed material that fed a dilute and turbulent shear flow.

Dynamic pressure, particle volumetric concentration, temperature and flow duration are hazardous characteristics of PDCs that can impact buildings and population and are defined here as impact parameters. They have been calculated by means of an implementation of the PYFLOW code, which uses the deposit particle characteristics as input. The software searches for the probability density function of impact parameters. The 84th percentile has been chosen as a safety value of the expected impact at long term (50 years). Maps have been constructed by interpolation of the safety values calculated at various points over the dispersal area, and show how impact parameters change as a function of distance from the volcano. The maps are compared with the red zone, which is the area that the National Department of the Italian Civil Protection has declared to be evacuated in the impending of an eruption. The damaging capacity of currents over buildings and population is discussed both for the highly concentrated part and the diluted one.

1 Introduction

Pyroclastic density currents (PDCs) originate from a variety of processes during explosive volcanic eruptions, e.g. the fountaining of the gas-particle mixture (aka eruption column) issuing from a crater or by the avalanching of a volcanic dome. In the first case, the parent current can evolve into a highly concentrated, massive underflow and an overlying, dilute, fully-turbulent current (Sulpizio et al., 2014). PDCs represent the most hazardous events of volcanic eruptions, with historic cases causing destruction and deaths over vast areas (Baxter et al., 1998; Cao et al., 2003; Sulpizio et al., 2014). Understanding the processes characterizing PDCs, such as transport and deposition of pyroclastic particles, from the study of deposits from PDCs is essential for developing effective hazard assessment and risk management strategies (Jones et al. 2023).

https://doi.org/10.5194/egusphere-2024-2971
Preprint. Discussion started: 9 October 2024

Various attempts have been made to define specific flow characteristics that are useful for evaluating the damaging capacity of PDCs, such as dynamic pressure, which is a measure of the impact force of a current that can solicit the resistance of buildings to lateral loads (Valentine et al., 1998; Spence et al., 2004; Zuccaro et al., 2008).

Other damaging factors are the flow temperature, the content of ash particles, and flow duration, which directly or indirectly affects the survivability of people caught unprotected by a PDC (Horwell and Baxter, 2006; Jenkins et al., 2013; Baxter et al., 2017). The latter become important especially over distal areas, where the mechanical strength of the current decays but the lethal effect of the gas-particle mixture remains, as it occurred at Pompeii during the historical eruption of 79 AD (Dellino et al., 2021), which represents an unvaluable source of information of the actual impact of PDCs.

No systematic analysis of these flow characteristics, which we define here as impact parameters, has been made so far for assessing quantitatively the hazard of a volcano. At Vesuvius, PDCs have been studied in previous papers (Sulpizio et al., 2007; Dellino et al., 2008; Sulpizio et al., 2010a; Mele et al., 2011; Dellino et al., 2021), but a detailed investigation of the impact parameters for the aim of a probabilistic hazard assessment is still not satisfactory.

PDCs at Vesuvius may be very dangerous, being the area surrounding the volcano highly populated, with around 700.000 inhabitants included in the red zone (Gurioli et al. 2010), which is the area to be evacuated in case of an impending eruption (Civil Protection Department, 2014). The red zone is undifferentiated as it concerns the effects that the PDCs could have on buildings or people. In this paper, we try to cover this gap and investigate the distribution of the impact parameters over the volcano's surroundings, including the red zone.

Since pyroclastic deposits are the only records left by PDCs at Vesuvius, deposits from past eruptions are the only way to get hints about the expected range of impact parameters. To follow this line, it is necessary to investigate the PDC deposits first, then define a general model of the current that links deposit characteristics to flow dynamics, and finally reconstruct the impact parameters that better represent flow intensity in terms of damaging potential. This is the way the paper is organized.

2 Reconstruction of the facies architecture of PDC deposits

Volcanism at Vesuvius, as reconstructed by deposit stratigraphy, dates back to around 39 cal. ky BP (Brocchini et al., 2001; Santacroce et al., 2008), with predominantly effusive eruptions forming the Monte Somma volcano. About 22 cal. ky BP, the activity changed into largely explosive eruptions, which formed the polyphased summit caldera of Mt Somma (Cioni et al., 1999). After Pompeii Plinian event of 79 AD, volcanism continued mainly within the Mt Somma caldera, with the formation of Mount Vesuvius. The last eruption occurred in AD 1944 (Cole and Scarpati, 2010).

The best preserved PDC deposits refer to the eruptions of Pomici di Mercato, 8.9 cal. ky BP (Santacroce et al., 2008; Mele et al., 2011), Pomici di Avellino, 3.9 cal. ky BP (Sulpizio et al., 2010b; Sevink et al., 2011), AP2, 3.5 cal. ky BP (Cioni et al., 2008), Pompeii (AD 79; Sigurdsson et al., 1985; Cioni et al., 1992), Pollena (AD 472; Sulpizio et al., 2005) and AD 1631 (Rosi et al., 1993). Other PDC deposits can be found in other eruptions (i.e. Pomici di Base and Greenish; Bertagnini et al., 1998; Cioni et al., 2003), but do not show the outcropping continuity necessary for the hazard analysis of the present research,

https://doi.org/10.5194/egusphere-2024-2971
Preprint. Discussion started: 9 October 2024

and are not considered here. According to Selva et al. (2022), there is a 34% probability of an eruption at Vesuvius in the next fifty years, which we consider as a reference time for the long-term hazard. Spotty data about input parameters have been published in the past using both geological data (Sulpizio et al. 2010a; Mele et al. 2011; Dellino et al. 2021) or numerical simulations (e.g. Neri et al. 2007; Esposti Ongaro et al. 2008), but a comprehensive indication of the expected intensity of PDCs in the Vesuvius area is still not available.

To take into account the whole eruptive history of Vesuvius, and to get an unbiased range of the variation of impact parameters, all the eruptions which show well-preserved deposits in the field are considered in this paper. This means that no particular event is used to propose a specific hazard scenario, but all the suitable PDC-forming eruptions are considered, in order to obtain a representative sample of the impact parameters of PDCs.

The field study, which extended from the gullies on the volcano flank to the plain surrounding Vesuvius, shows that a PDC deposit is composed of a sometime repetitive succession of beds in stratigraphic continuity. Combining observations of all deposits, a general “facies architecture” has been defined, synthesizing the lateral and vertical succession of beds associated with a current (Figure 1). The general facies architecture well represents the common behaviour of PDC emplacement at Vesuvius, and is the base for the PDC emplacement.

https://doi.org/10.5194/egusphere-2024-2971
Preprint. Discussion started: 9 October 2024

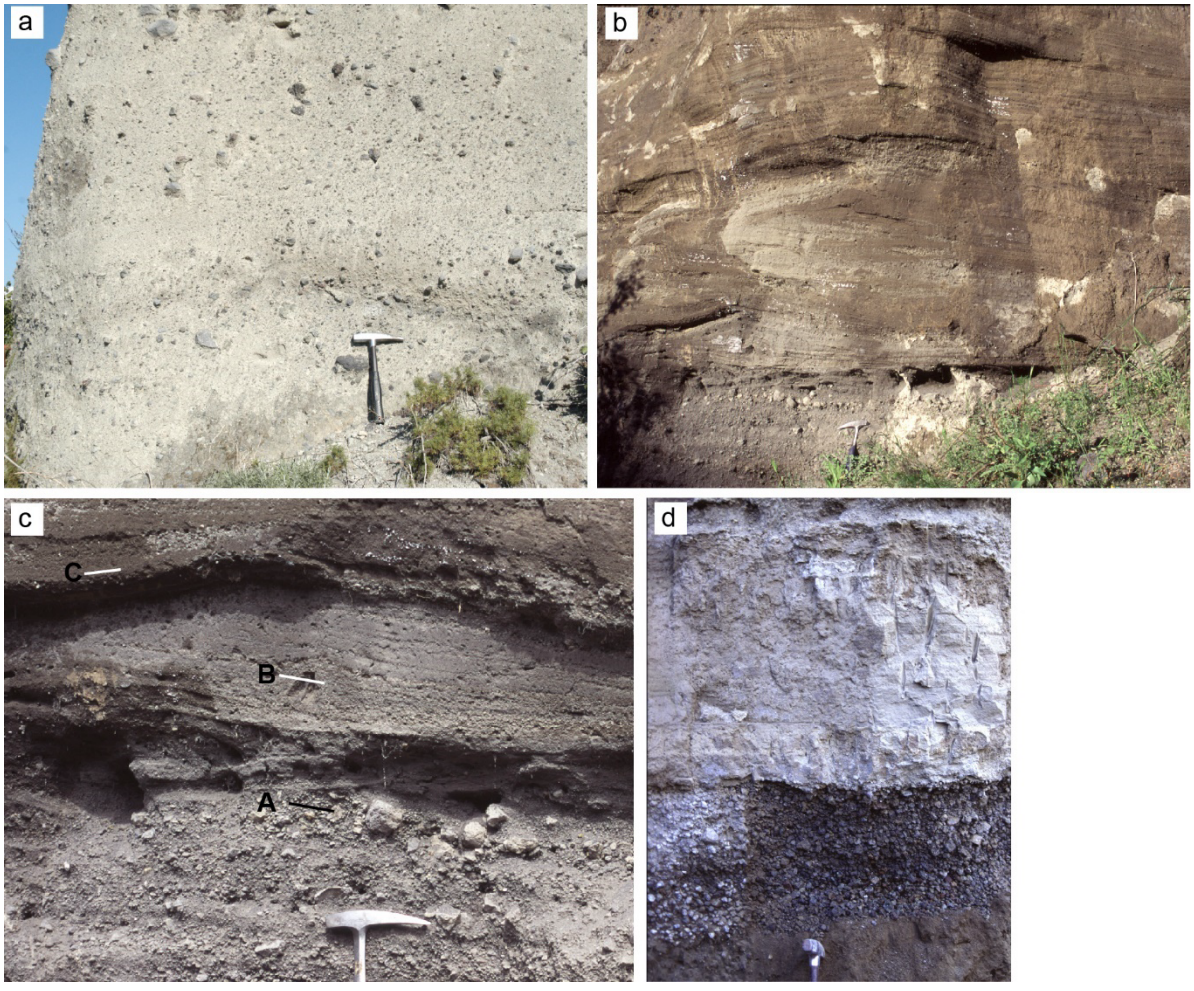

Figure 1. Deposits of pyroclastic density currents at Vesuvius. a) a massive, structureless deposit of ash, lapilli and bombs. b) a decimeter to meter thick dune-bedded layer of ash and lapilli with internal lamination and traction structures. c) the fining upward succession formed by the passage of a PDC: A = coarse clast entrained at the base of the current. The clast is 7 cm long. B = laminated layer. C = thin, fine ash layer. d) Fine-ash deposit.

In the proximal area, along the gullies that cut the volcano slope, the vertical facies architecture is generally composed of meters thick poorly-sorted massive layer of ash, lapilli and bombs (Figure 1a). It is followed by a decimetre to meter thick stratified, sometimes dune-bedded bed of ash and lapilli with internal lamination and traction structures (Figure1b, c). The facies architecture is closed by fine-grained ash layer(s) of centimetric thickness (Figure1c). Coarse grained massive facies occur close to the break in slope between the volcano and the surrounding apron, at the mouth of the main valleys draining the volcano slopes. Stratified facies predominate in overbank deposits, and, for Avellino and Pompeii eruptions also beyond the break-in slope up to the distal area (tens of km from the volcano). As a general rule, the stratified facies decreases in thickness and grain size with distance from the source, while the fine-grained ash facies remains almost constant in grain size (Figure1d).

https://doi.org/10.5194/egusphere-2024-2971
Preprint. Discussion started: 9 October 2024

The facies cropping out along the gullies are the result of a basal highly-concentrated underflow, which forms the massive facies, and an overlying dilute current, forming the stratified facies and the fine-ash one. The contemporaneous occurrence of a massive underflow together with a dilute overcurrent has already been reported (Druitt et al., 2002; Gernon et al., 2013; Breard and Lube, 2017). This deposit architecture can be interpreted in terms of a current that in its early phase of development was separated into two parts, depending on a different balance between the sedimentation rate and shear rate (i.e. the bedload transportation capacity of the current).

Our interpretation is that the massive layer was fed directly from the impact of the pyroclastic fountain or column collapse to the ground, which was characterized by a high sedimentation rate that dumped turbulence due to a high particle concentration. It has already been demonstrated that thick, massive deposits can be formed directly from suspension, because of a high sedimentation rate, also called suspended-load fallout rate, which inhibits traction at the bedload (Lowe, 1982, 1988; Fisher, 1990; Druitt, 1992; Kneller and Branney, 1995; Branney and Kokelaar, 2002; Woods et al., 2002; Postma et al., 2009). Furthermore, experiments show that massive beds are formed from suspension where the sedimentation rate exceeds the bedload transportation rate by two orders of magnitude (Dellino et al. 2010; 2019).

The underflow was channelised along the volcano valleys and stopped abruptly at the break-in slope (Figure 1a).

The lateral stress generated by the impact of the collapsing column on the ground led to the "squeezing" (fluidization) of part of the collapsed material and fed an overlying shear flow decoupled from the massive flow (Dellino et al. 2020). It evolved laterally into a highly expanded, fully turbulent, gas-particle current that formed both the stratified facies (Figure 1b,c) and the fine-grained ash from gentle settling of the suspended material during the waning phase of the current. It has a long time of sedimentation trough the atmosphere, and can be easily drifted away from lower atmosphere winds over the plain surroundings the Vesuvius.

3 Physical modelling of impact parameters: the example from the Mercato eruption

Before showing the hazard maps obtained by integrating data from all eruptions, the approach used in the reconstruction of the impact parameters is illustrated by the example of one PDC of the Pomici di Mercato eruption.

The stratigraphy of the Pomici di Mercato eruption (Mele et al., 2011) is made up of alternating fallout and PDC deposits that are well-exposed in the northern sector of the volcano (Figure 2a). The PDC deposits considered here are from the first phase of the eruption and consist of a meter-thick poorly-sorted massive layer of lapilli and scattered bombs and blocks set in an ash matrix (Figure 2b, c), which is related to the highly-concentrated underflow, and a dune-bedded, stratified layer (Figure 2c, d), which is related to the overlying dilute current. When cropping out on the gentle slope of the volcano flank, the stratified layer shows a thickness of 0.5 m and small dunes of lapilli and ash of 1 m wavelength and 0.1 m in height (Figure 2c).

The physical characteristics of the bipartite current need to be to reconstructed by means of two separate models.

https://doi.org/10.5194/egusphere-2024-2971
Preprint. Discussion started: 9 October 2024

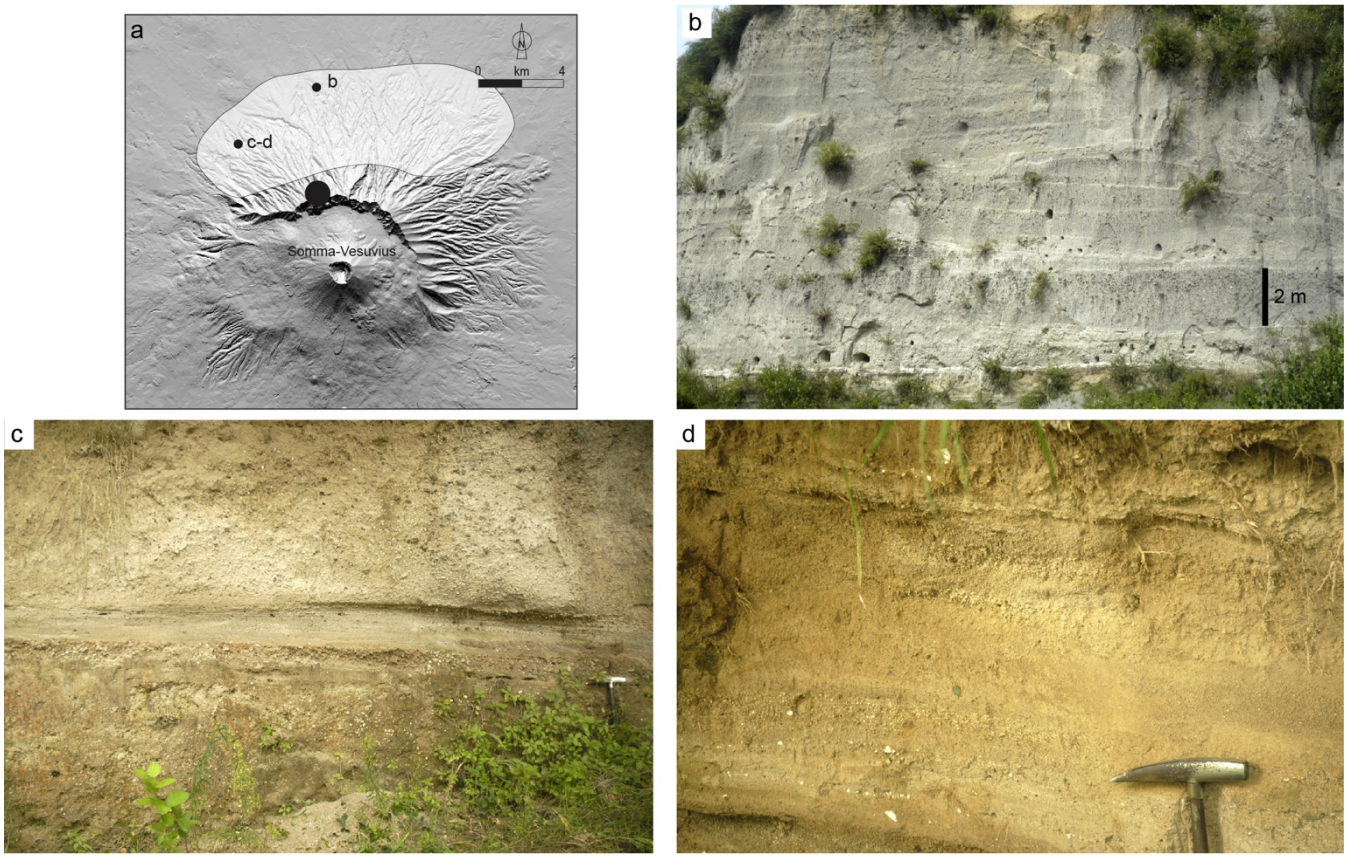

Figure 2. Field pictures showing the Mercato eruption deposits used as a case study. (a) The labels b, c and d refer to the deposits shown in b, c and d. The black circle represents the zone of impact of the eruptive fountain (the digital elevation model by Tarquini et al., 2023). The white shaded area represents the dispersal area of the PDCs. (b) The massive deposit emplaced by freezing at the break in slope. (c) The stratified layer at the base of the massive layer at the split location. Structure spacing is about 1.0 m, height about 0.1 m. (d) The stratified layer on top of the massive layer at the split location.

In the following, the model of the overlying dilute current, which represents the deposition of the dune-bedded layer, is discussed first. Afterward, the model of the highly-concentrated undercurrent forming the massive bed, is presented. Such an order of illustration is motivated by the fact that data from the overlying current help constraining the flow model of the underlying one.

3.1 Model of the overlying dilute current forming the dune-bedded layer

The overlying dilute current, which formed the stratified dune-bedded layer, is modelled as a turbulent boundary shear flow (Furbish, 1997; Dellino et al., 2008) that takes solid particles into suspension. Flow movement is initiated by the shear stress acting on the volcano slope, which is due to the density difference between the volcanic gas-particle mixture and the surrounding atmosphere. The current is made up of a mixture of magmatic gas, volcanic particles, and atmosphere-air entrained

https://doi.org/10.5194/egusphere-2024-2971
Preprint. Discussion started: 9 October 2024

by turbulence during runout. It is stratified in terms of velocity and particle concentration, hence density (Middleton and Southard, 1984; Valentine, 1987). As a consequence of sedimentation and air entrainment, the volumetric particle concentration decreases down to a point where the density difference with atmosphere is nullified and the current stops its lateral movement and becomes buoyant. The final deposition from the buoyant part of the current forms the fine-ash layer that closes the layer sequence.

The distribution of particles of different sizes in the deposit layering, suggests that a link exists between current flow dynamics and particle attitude to be first taken into suspension, then to sedimentation, and finally by traction on the ground. Such a link allows the use of particle characteristics (size, density and shape), as measured in the laboratory on sediment samples, for constraining the flow model and calculate the impact parameters. A detailed formulation of the physical model (Dellino et al., 2008) and of the numerical software code PYFLOW v2.5 (Dioguardi and Dellino, 2014; Dioguardi and Mele, 2018) is deferred to Appendix A. The main data used as input are reported in the Zenodo repository (Mele et al. (2024)).

Since model solutions depend on particle characteristics (mainly grain size, density and aerodynamic coefficients) and since deposits are characterized by a broad distribution of particle size and densities, solutions of impact parameters are given in terms of a Probability Density Function (PDF), which depends on the statistic distribution of deposit particles characteristics. The 84th percentile is considered here as a safety value for evaluating the damaging effect of the impact parameters.

In the following, the results of flow dynamic pressure, particle volumetric concentration, temperature, and flow duration, representing the impact parameters, are illustrated for the study case of the Pomici di Mercato eruption.

3.1.1 Flow dynamic pressure and particle volumetric concentration

In order to illustrate how flow characteristics vary in the stratified current, the profiles of particle concentration, density, velocity, and dynamic pressure are shown in Figure 3. Results are presented by means of the 84th, 50th and 16th percentile of the PDF, which were calculated with the method of Dioguardi and Dellino (2014; see the method in Appendix A) and show the statistic variability in terms of percentiles.

https://doi.org/10.5194/egusphere-2024-2971
Preprint. Discussion started: 9 October 2024

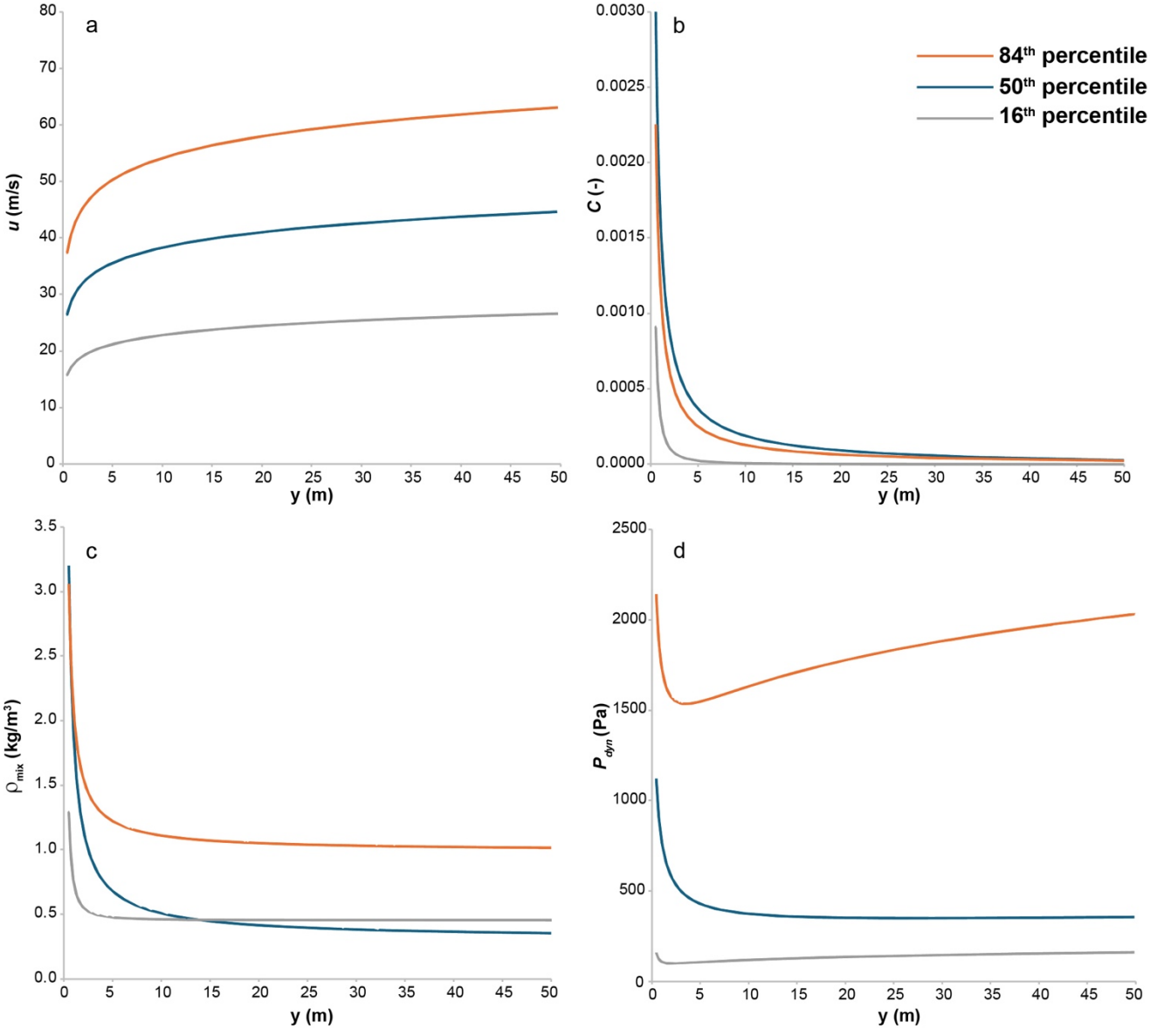

Figure 3. Profiles of the impact parameters representing the flow dynamic pressure. The curves refer to the minimum (16th percentile), the average (50th percentile) and the maximum (84th percentile) of the probabilistic model solution. (a) Velocity profiles. (b) Particle volumetric concentration profiles. (c) Density profiles. (d) Dynamic pressure profiles.

Velocity (u) logarithmically increases upward in the flow (Figure 3a), reaching values in the range of tens m/s (a list of symbols is provided in Table 1). Particle volumetric concentration (C) decreases with height (Figure 3b), and already in the first few meters is lower than 0.001. The density profile (ρ_{mix}) mimics the trend of the concentration profile (Figure 3c), and rapidly decreases down to a value lower than atmosphere, making the upper part of the current buoyant. The dynamic pressure P_{dyn}

https://doi.org/10.5194/egusphere-2024-2971
Preprint. Discussion started: 9 October 2024

has a maximum in the first few meters (Figure 3d). Higher in the current, dynamic pressure ranges around 1 kPa. The P_{dyn} value integrated over the first 10 m of the current, which we consider helpful for representing the stress acting on a typical building, is 1.7 kPa. With such a value, moderate mechanical damages are expected (Zuccaro et al., 2008; Zuccaro and Leone, 2012).

Table 1. Notation

Symbol	Description	Units
A_r	Aggradation rate	m s^{-1}
C	Particle volumetric concentration	-
C_0	Reference particle concentration in the Rouse equation	-
C_d	Drag coefficient	-
C_{ga}	Volumetric concentration of the entrained air	-
$C_{ga,rel}$	Relative volumetric concentration of the entrained air	-
C_{gm}	Volumetric concentration of the magmatic gas	-
$C_{gm,rel}$	Relative volumetric concentration of the magmatic gas	-
Cp_m	Specific heat at constant pressure of the magmatic gas	J kg^{-1} K^{-1}
Cp_s	Specific heat at constant pressure of the particles	J kg^{-1} K^{-1}
d	Particle size	m
d_{ent}	Entrained particle size	m
g	Gravity acceleration	m s^{-2}
H_{dep}	Total deposit thickness	m
H_{lam}	Thickness of the laminated layer	m
k	Von Karman's constant	-
k_s	Substrate roughness	m
P_{dyn}	Dynamic pressure	Pa
P_n	Particle Rouse number	-
$P_{n,avg}$	Average Rouse number of the particles in the current	-
$P_{n,susp}$	Average Rouse number of particles in turbulent suspension	-
P_n^*	Normalized Rouse number of the current	-
P_{ni}	Rouse number of the i^{th} solid fraction in the deposit	-
R_a	Specific gas constant of air	J kg^{-1} K^{-1}
Re_*	Particle Reynolds number	-
R_m	Specific gas constant of the magmatic gas	J kg^{-1} K^{-1}

https://doi.org/10.5194/egusphere-2024-2971
Preprint. Discussion started: 9 October 2024

S_r	Sedimentation rate	kg m^{-2} s^{-1}
T	Flow temperature	K
t	Time of deposition	s
T_a	Air temperature	K
T_m	Temperature of the magmatic gas	K
T_s	Particle temperature	K
u	Velocity	m s^{-1}
u_*	Shear velocity	m s^{-1}
w_t	Particle settling velocity	m s^{-1}
z	Vertical coordinate	-
z_0	Reference height in the Rouse equation	m
z_{sf}	Shear flow thickness	m
z_{tot}	Total flow thickness	m
α	Substrate slope	°
θ	Shields parameter	-
μ	Fluid viscosity	Pa s
ρ_{atm}	Atmospheric density	kg m^{-3}
ρ_g	Gas density	kg m^{-3}
ρ_{mix}	PDC flow bulk density	kg m^{-3}
ρ_s	Particle density	kg m^{-3}
$\rho_{s,ent}$	Entrained particle density	kg m^{-3}
ρ_{si}	Density of the ith solid fraction in the deposit	kg m^{-3}
τ	Flow shear stress	Pa
τ_0	Yield strength	Pa
ϕ_i	Weight fraction of the ith solid fraction in the deposit	-
ρ_{dep}	Deposit density	kg m^{-3}

175

3.1.2 Flow temperature

Flow temperature was calculated by using as input in eq. (A13; see the appendix A) the values of density, concentration, temperature and specific heat of the three components of the gas particle mixture, namely: magmatic gas, air and volcanic particles. The temperature of magmatic gas T_m and of volcanic particles was set to 850 °C, which is compatible with the
180 temperature of Vesuvius magmas (Cioni et al. 2004). Average density was set to 1700 kg m^{-3} for the volcanic particles, to 0.2 kg m^{-3} for volcanic gas at 850 °C and to 1.2 kg m^{-3} for air at 18 °C, respectively. The specific heats were set to 2200 J kg^{-1} K^{-}

https://doi.org/10.5194/egusphere-2024-2971
Preprint. Discussion started: 9 October 2024

[1] for volcanic gas, 700 J kg^{-1} K^{-1} for the volcanic particles and 1005 J kg^{-1} K^{-1} for air. As for the particle concentration, an average value of 0.001 was set, which was obtained by integrating the concentration profile over flow height at 10 meters (see Figure 3b) by means of Eq. (A7). The relative concentrations of air and magmatic gas were obtained by means of the method illustrated in Appendix A and resulted as 0.941 and 0.058, respectively. A temperature about 500 °C was obtained, in the first few meters of the current, by solving Eq. (A17).

The low temperature obtained in the distal areas is due to the very low content of solid particles and a high content of cold atmosphere air in the current, which is attributed to the air entrainment process that characterizes PDCs along runout.

3.1.3 Flow duration

Flow duration was calculated by dividing layer thickness (H_{dep}) by the sedimentation rate (S_r). The method is described in Appendix A. The input data: particle concentration, Rouse number and settling velocity, are all functions of the shear flow density, which was calculated in terms of a PDF with PYFLOW v2.5 (Dioguardi and Mele, 2018). As a consequence, also flow duration is expressed in terms of probabilities. The average value of flow duration was about 20 min at section 14 of Fig.2, representing the case study of Mercato eruption. The duration is quite long when compared to the couple of minutes considered as a survivable time for people engulfed in a PDC, even at low temperature (Horwell and Baxter, 2006; Baxter et al., 2017).

3.2 Model of the highly concentrated undercurrent that formed the massive bed

In order to constrain the general model of the basal part of PDCs that forms the massive deposits, we can start from the experimental data on granular flows of volcanic material passing over a break in slope (Sulpizio et al. 2016). The method was successfully tested against granular avalanches of 1944 eruption at Vesuvius and for some of the volcaniclastic flows occurred on May 5-6, 1998, in the Sarno area. In particular, Sulpizio et al. (2016) provided an equation linking velocity and distance travelled beyond the break in slope, using different slope ratios:

$$\frac{v}{v_{max}} = 1 + m\mathrm{D} + n\mathrm{D}^2 + p\mathrm{D}^3 \quad (1)$$

where v_{max} is the velocity at break in slope, D is the distance beyond the break in slope, and m, n and p are parameters depending by ΔH, defined as the difference in height between the source area and the front of the deposit:

$$\begin{cases} m = \frac{a}{\Delta \mathrm{H}} \\ n = \frac{b}{\Delta \mathrm{H}} \\ p = \frac{c}{\Delta \mathrm{H}} \end{cases} \quad (2)$$

https://doi.org/10.5194/egusphere-2024-2971
Preprint. Discussion started: 9 October 2024

where a, b and c are parameters depending on the slope ratio (SR), defined as the ratio between the slope downvalley and upvalley of the break in slope:

$$\begin{cases} -a = 4.91e^{-2.1SR} \\ b = 15.56e^{-3.51SR} \\ -c = 16.73e^{-4.88SR} \end{cases} \quad (3)$$

In order to get the velocity at different distances beyond the break in slope we have to set ΔH and v_{max}. For the case under study, the height of impact on the ground of the collapsing pyroclastic material was set around 800-900 m and the height of deposits occurrence was set around 200-300 m, which resulted in a ΔH of 600-700 m. The velocity at the break in slope can be set around 15 m s^{-1}, similar to that measured for volcaniclastic flows of May 5-6, 1998 in the Sarno area (Zanchetta et al. 2004). The present-day SR around Vesuvius is close to 0.5, which has been used as input value in equation (3). Figure 4 shows the results for a DH of 600 m. It is worth noting that the deposit distance for SR=0.5 is around 800-900 m, quite in agreement with the field data (Gurioli et al. 2010).

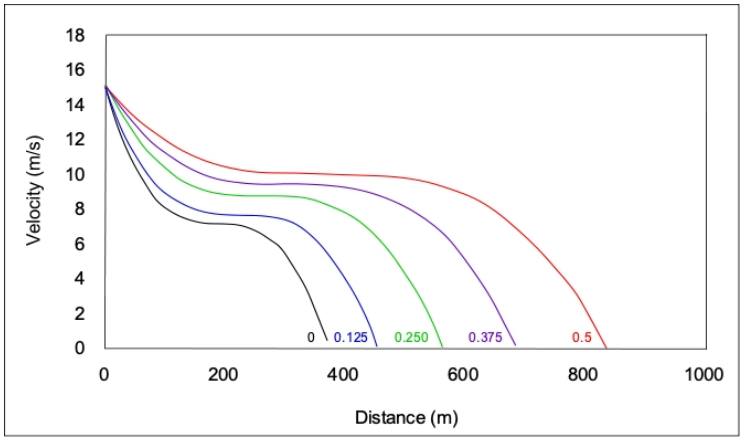

Figure 4 .Velocity profiles beyond the break in slope for different SR.

In order to constrain the specific flow model of the massive undercurrent of Mercato eruption, we used data from the stratified layer formed by the overlying current. When cropping out on the gentle slope of the volcano flank, the stratified layer is 0.5 m thick. When it occurs along the steeper slopes of the gullies departing from the crater rim, it is split into two parts by the intercalated massive layer of the underflow. The split consists of a 0.15 m thick basal part (Figure 2c) and a 0.35 m thick top

https://doi.org/10.5194/egusphere-2024-2971
Preprint. Discussion started: 9 October 2024

part (Figure 2d). The intercalated massive layer is 1.6 m thick (Figure 2c). The different speeds of the two flows moving downslope justify such interpenetrating stratigraphy between the massive and the dune-bedded layer. The dilute current, being faster, overtook the slower basal flow and started forming the dune-bedded layer by aggradation. After the massive flow passed over, the aggradation of the dune-bedded layer continued as long as the current was fed from the source. This kind of sandwiching stratigraphy is quite common for sedimentary deposits, as reported for turbidites (e.g., Talling et al., 2004).

The speed of the underflow can be estimated by the ratio between the distance from the crater rim and the total time the underflow took to reach the dune-bedded layer at the 'split' location. The total time is evaluated by summing the time the overcurrent took to reach the 'split' location plus the time that the overcurrent took to accumulate, by aggradation, the part of the stratified layer found under the massive one (0.15 m). The former time, 95 sec, was calculated by the distance, 4 km, divided by the speed of the overcurrent, ca 42 m s^{-1}, which was calculated by means of the turbulent boundary-layer shear flow approximation (Eq. (A6)) using PYFLOW v2.5 (see sample 13/4, in Table 2 and Mele et al. (2024)). With the software, the time of aggradation of the stratified layer found under the massive layer was calculated, and resulted in 1140 sec. The total time that the underflow took to reach the split location was 1235 sec, corresponding to a velocity of the massive undercurrent of 3.23 m s^{-1}, which is much slower than that of the overcurrent, as expected for a highly concentrated massive flow moving downslope, and in good agreement with the range of Figure 4.

The massive facies stops at the base of the volcanic cone where, as a consequence of the decrease of the slope angle, it freezes in a 2 m thick layer (Figure 2b). Such a behaviour is typical of flows with a high internal yield strength that does not allow downslope flowage until a minimum shear stress is overcome, similarly to a Bingham-plastic (Furbish, 1997). Such flows stop when the slope decreases and the yield strength equals shear stress. Assuming that flow density was not much different from that of deposit, i.e., 1400 kg m^{-3} (as calculated by considering a known volume of deposits and weighing it), the yield strength τ_0 can be equated to the shear stress acting on the slope, which results in the minimum stress for the down-slope movement of the massive flow:

$$\tau_0 = \rho_{dep} g \sin \alpha H_{dep} \quad (1)$$

With a slope angle α of 1.5° and a deposit thickness H_{dep} of 2 m, the yield strength is 700 Pa.

By inverting the equation of the height-averaged velocity of a Bingham-plastic;

$$\overline{u(z)} = H\left(\frac{\rho_{dep} g \sin \alpha H}{3\mu} - \frac{\tau_0}{2\mu}\right) \quad (2)$$

and using the value of yield strength τ_0 previously obtained, the thickness H of the massive layer, and a slope angle at the 'split' location of 6.5°, a viscosity μ of 200 Pa s results, which completes the rheological characterization of the massive underflow. Such a rheology is compatible with other massive sedimentary flows, to which massive pyroclastic flows have already been compared in the literature (Fink et al., 1981; Major and Pierson, 1992; Palladino and Valentine, 1995; Major and

https://doi.org/10.5194/egusphere-2024-2971
Preprint. Discussion started: 9 October 2024

Iverson, 1999; Capra et al., 2018). While such type of flows maintain mobility only inside channels and stop at the gully apron, they are still destructive at the foot of the volcano because of a dynamic pressure over of 7 kPa, and high temperature, which is due to the high particle concentration.

4 Hazard maps and expected impact

The impact parameters of the PDCs were reconstructed from the deposits of all eruptions that showed, in the field, a good enough exposure to both characterize the deposit structure and to sample the pyroclastic material for the laboratory analyses. Multiple deposits cropping out along the dispersal area were investigated for each eruption. A list of the locations of the deposits' taken into analysis is provided in Table 2 and a map is displayed in Figure 5. The input and output files of all the PYFLOW simulations for each deposit is provided in Mele et al. (2024). The models used in the PYFLOW code for calculating the impact parameters are the same as those illustrated in the previous section's example of the Pomici di Mercato eruption and explained in more detail in the Appendix A.

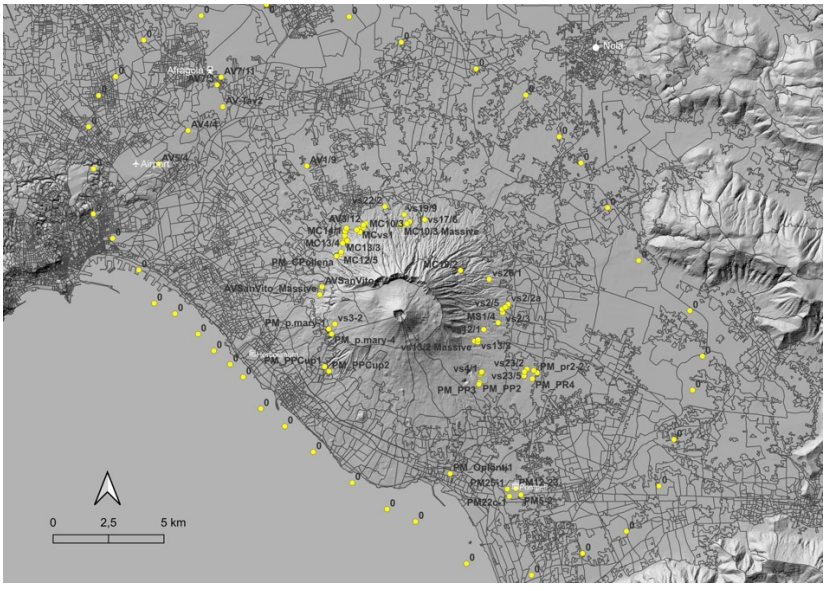

Figure 5. Map of sample locations at Vesuvius (see Table 2 for more details). The digital elevation model (Tarquini et al., 2023), territorial bases and census variables (Istat, 2011) are used as the topographic base for data set visualizations.

Table 2. List of the sample locations (cartographical reference system WGS 84-UTM 33N.

Eruption	Unit	sample	X (m)	Y (m)
AD 1631	1631	MS1/4	456008.13	4518724.03

https://doi.org/10.5194/egusphere-2024-2971
Preprint. Discussion started: 9 October 2024

(Rosi et al., 1993)				
	S1	vs17/6	452734.67	4523363.56
	S1	vs19/9	451810.00	4523595.88
	S1	vs22/2	450944.56	4523960.21
	S1	vs2/1	456416.53	4519450.54
	S1	vs4/1	455205.03	4516400.34
	S2	vs23/5	457160.09	4516331.52
	S2	vs2/2a	456466.04	4519547.75
	S2	vs4/3	455224.57	4516447.74
	S2	vs23/2	457284.24	4516635.62
Pollena (AD 472)	S2	vs13/2 Massive	454938.93	4517904.16
(Sulpizio et al., 2005)	S2	vs13/2	455088.76	4517858.92
	S2	vs2/3	456213.00	4519171.41
	S2	vs12/1	455358.48	4518422.88
	S2	vs23/4	457179.51	4516514.30
	Sy	vs26/1	455613.39	4520674.32
	Sy	vs4/6	455228.34	4516482.65
	Sy	vs2/5	456186.41	4519330.02
	Sy	vs13/3	455098.74	4517964.11
	Sy	vs4/5	455252.46	4516521.57
	Sy	vs2/4a	456327.61	4519414.50
	EU3pf	PM_PP2	455153.96	4516044.29
	EU3pf	PM_pr2-2	457748.39	4516468.36
	EU3pf	PM_pr2	457596.00	4516572.87
	EU4	PM_PP3	455125.20	4515969.86
	EU4	PM_p.mary-1	448383.07	4518488.93
Pompeii (AD 79)	EU4	PM_PR4	457532.66	4516201.35
(Cioni et al., 1992)	EU4	PMvs1_Massive	449818.91	4522825.06
	EU4	PMvs1	449669.96	4522919.38
	EU4	PM_Oplonti1	453805.10	4511968.91
	EU4	PM_CPollena	448750.75	4521753.94
	EU4	PM_PPCup1	448182.52	4516805.40
	EU4	PM_PPCup2	448379.34	4516597.53

https://doi.org/10.5194/egusphere-2024-2971
Preprint. Discussion started: 9 October 2024

	EU4	PM5-2	456987.12	4511000.96
	EU4	PM25-1	456374.22	4511259.25
	EU4	PM22c-1	456467.72	4510935.56
	EU4	PM12-23	456757.24	4511281.08
	EU7	PM_p.mary-4	448507.65	4518263.67
AP2 (Cioni et al., 2008)	AP2	vs3-2	448658.59	4518710.98
Pomici di Avellino (Sulpizio et al., 2010)	EU5 a	AV2/2	449209.95	4522930.73
	EU5 b	AV2/5	449142.01	4522869.39
	EU5 b	AV2/7	449208.65	4523011.56
	EU5 b	AV1/9	447451.73	4525799.95
	Cava San Vito	AVSanVito_Massive	447987.83	4520035.70
	Cava San Vito	AVSan Vito	448091.94	4520384.36
	EU5 b	AV_Tav2	443690.19	4528476.65
	EU5 b	AV4/4	442120.93	4527426.14
	EU5 b	AV5/4	440790.89	4525942.00
	EU5 b	AV7/3	443439.30	4529463.26
	EU5 c	AV7/11	443623.49	4529801.35
	EU5 c	AV3/12_Massive	449968.79	4523028.51
	EU5 c	AV3/12	449978.44	4523138.63
Pomici di Mercato (Mele et al., 2011)	EU4	MCvs1	449777.76	4522964.23
	EU4	MCvs2	450072.39	4523203.00
	EU4	MC13/3	449064.39	4522395.94
	EU4	MC8/3	452056.53	4523272.95
	EU4	MC10/3	451918.93	4523181.88
	EU4	MC10/3 Massive	451662.41	4523113.25
	EU4	MC14/1	449126.76	4522613.68
	EU4	MC14/2	449129.16	4522678.89
	EU4	MC19/2	454328.68	4521073.78
	EU6	MC13/4_Massive	449242.12	4522437.32
	EU6	MC13/4	449036.04	4522328.96
	EU6	MC12/5	448943.77	4521846.17
	EU8	MC12/7	448965.37	4521944.05

https://doi.org/10.5194/egusphere-2024-2971
Preprint. Discussion started: 9 October 2024

Upon processing data with the PYFLOW code, only results that were significant after a t-test on grain size, at 5% probability, were included in the final database (see PYFLOW user manual for more details). The resulting dataset consists of 65 georeferenced data points distributed around the volcano, each containing values of the four impact parameters: dynamic pressure, particle volumetric concentration, temperature and flow duration. The 84th percentile of the PDF, which we consider as a safety value of the intensity of PDCs, is used for constructing the hazard maps.

By the analysis of data shown in Figure 6, which are arranged in order of eruption age, no temporal trend of PDC intensity (as expressed here by the dynamic pressure) emerges at Vesuvius. The variability inside an eruption (between different PDCs) covers a broad range as it is also the variation of parameters among eruptions. Therefore, there is no reason to choose one specific eruption as representative of the hazard of PDCs, which, in the long term, means in the next fifty years. It is also to note that if one considers the scale of eruptions as represented by the total volume of volcanic material emitted (which also includes deposits of other origin with respect to PDCs, such as Plinian fallout), which is an often used metric in Volcanology, there is not any correlation between eruption size and PDC intensity. This is likely to be related to the fact that the material erupted during a single PDC is a very small fraction of the total eruption volume, and still, each current is very dangerous. An example is the Pollena eruption, whose PDCs are not weaker than those of Mercato or Pompei, but have a total volume 5 times smaller (Sulpizio et al., 2005; 2007).

https://doi.org/10.5194/egusphere-2024-2971
Preprint. Discussion started: 9 October 2024

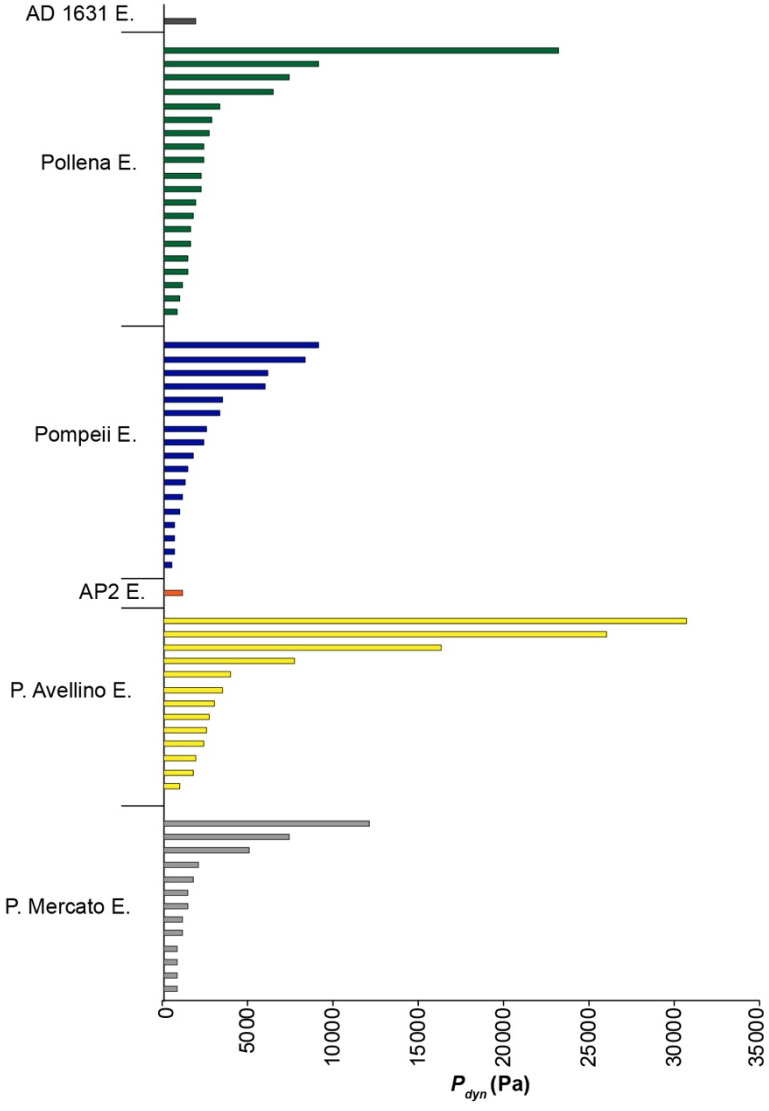

Figure 6. Dynamic Pressure (Pa) values (over the first 10 m of the current), calculated from the deposits of all studied eruptions.

All data points of all eruptions have been, therefore, used for drawing the hazard maps, without any choice of a particular case as a specific scenario to be expected in the long term.

Hazard maps representing the isolines of the expected safety values of the impact parameters are shown in Figure 7. The maps were produced using the open source QGIS software. To reconstruct the maps, it was first necessary to add "zeroes" (zero values of impact parameters), representing points where PDC deposits do not crop out. Then we applied the QGIS contour plugin in order to spatially interpolate the data (Crook and Rouberyrie, 2024). Each map of Figure 7 represents one impact

https://doi.org/10.5194/egusphere-2024-2971
Preprint. Discussion started: 9 October 2024

parameter. Also, data were rasterized based on a regular grid at 250 m resolution, and are provided in the Zenodo repository (Mele et al. 2024), which could be useful for vulnerability analysis.

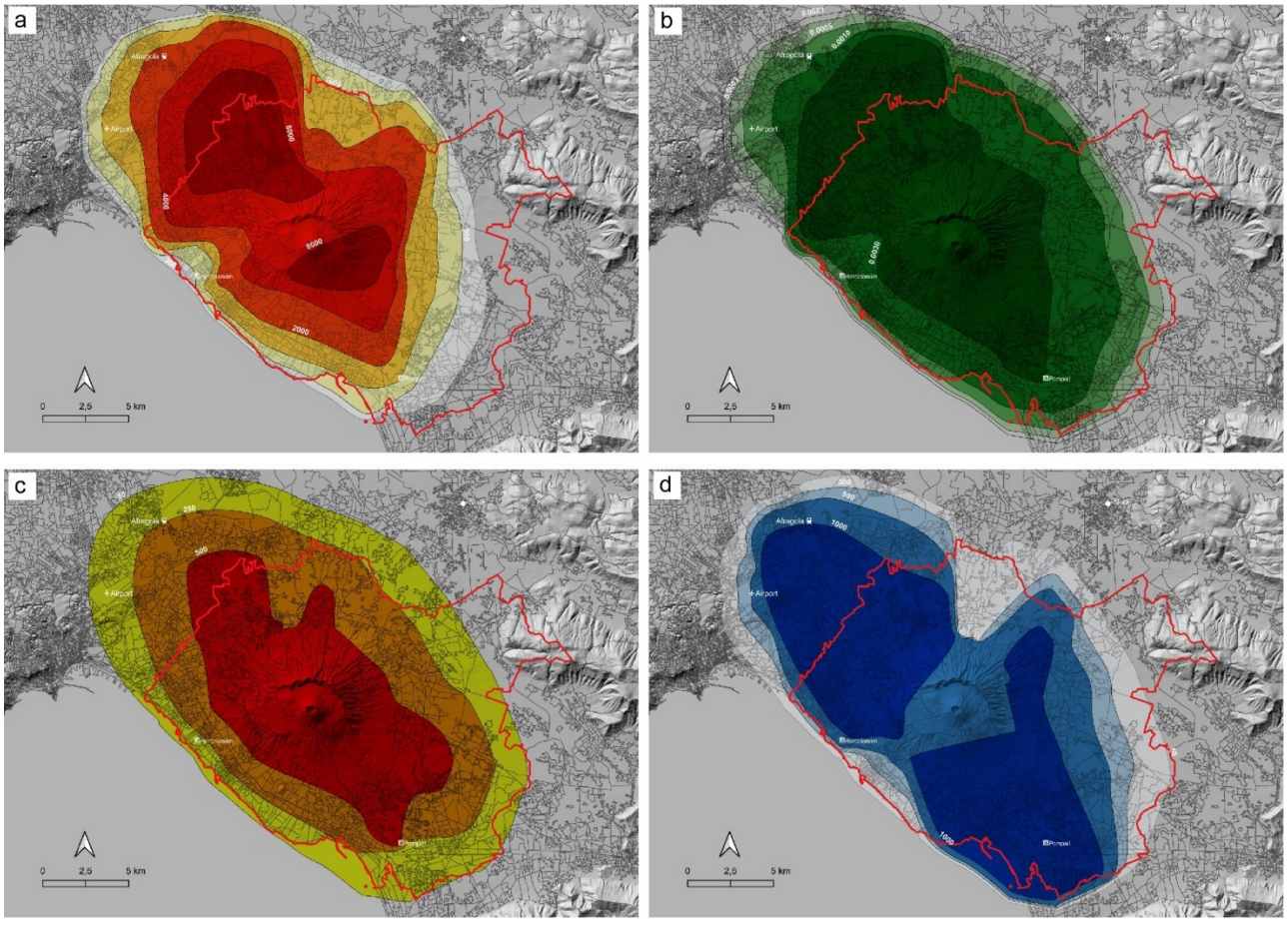

315 **Figure 7. Hazard maps of pyroclastic density currents at Vesuvius. The red solid line represents the boundary of the red zone proposed by the Italian National Civil Protection Department (2014). a) Dynamic Pressure (Pa) integrated over the first 10 m of the current. b) Particle volumetric concentration integrated over the first 2 m of the current. c) Flow temperature (°C) in the first 2 meters of the current. d) Average flow duration (s). The digital elevation model (Tarquini et al., 2023), territorial bases and census variables (Istat, 2011) are used as the topographic base for data set visualizations.**

320

From all the maps a decrease of PDCs intensity emerges as a function of the distance from the volcano, which helps differentiating the potential impact of PDCs over the territory with respect to the undifferentiated red zone proposed by the National Civil Protection Department of Italy (Civil Protection Department, 2014) , which is delineated on the maps in Figure 7 by the red solid line. Our maps tend to cover quite well the extension of the red zone, the only exception being the northwest 325 area, where the maps extend a little further than the red-zone limit. This is because our maps include the PDCs of the Avellino eruption, which spread over northwest but were not used in the drawing of the red-zone map because they were considered as

https://doi.org/10.5194/egusphere-2024-2971
Preprint. Discussion started: 9 October 2024

representative of a too big scenario. On the contrary, they were included in our study because, as discussed earlier, we do not choose any particular scenario as representative of the hazard in the long term, but consider the PDCs of all eruptions.

Our maps, by including intensity information, allow us inferring the potential impact of PDCs on buildings and the population, and could serve as a constraint for projecting the mitigation actions in the different areas around the volcano.

A constraint to the flow mobility exists toward northeast, which is represented by the remnants of Monte Somma, while toward southwest there is the sea, which is not considered in the red zone.

At the centre of the maps, around the Vesuvius cone, the massive undercurrents occur and result in high values of impact parameters, with dynamic pressure over 8 kPa (Figure 7a) and temperature over 500°C (Figure 7c), caused by the high particle concentration. These flows are totally destructive and do not allow, to our knowledge, to project any sustainable structural action for protecting buildings or populations (aside from evacuation). This conclusion is supported by data at Herculaneum, where the massive flows of the Pompeii eruption left a massive deposit that caused the breaking of thick Roman walls and charred woods (Giordano et al. 2018). Results of the calculations for the massive undercurrents in the locations, where it has been possible to apply the model of section 3.2, are provided in the Zenodo repository (Mele et al. 2024).

Moving away from the cone, the isolines of the impact parameters refer to the overlying dilute currents, since the massive underflow stops at the base of the volcano. Values of the impact parameters vary significantly moving away from Vesuvius, implying a different impact in the various zones around the volcano.

Concerning the impact over buildings, dynamic pressure (Figure 7a) shows values even over 8 kPa in the more proximal zones, both toward northwest and southwest, while they reduce to less than 1 kPa at the margin of the red zone. This is due to the decrease of both speed and concentration. Engineering investigations (Spence et al., 2004; Zuccaro et al., 2008; Zuccaro and Leone, 2012) show that values higher than 5 kPa can significantly damage buildings, while pressure under 1 kPa has minimal to no consequence on structures or infrastructures. Different impacts can be indeed expected on buildings as one moves away from the volcano, and while in proximal areas severe damages are expected, on distal locations, such as Pompeii, 10 km from the volcano, the mechanical effects of the dilute currents strongly decrease down to a value lower than 1 kPa. No damage to walls should be expected with such a flow strength (Spence et al., 2004; Zuccaro et al., 2008; Zuccaro and Leone, 2012), which is consistent with the fact that at Pompeii, during the 79 AD eruption, the walls of Roman buildings do not show evidence of damage (Luongo et al., 2003; Gurioli et al., 2007) related to the passage of the PDC. While this is not the proper place to discuss in detail the engineering actions that can be used for protecting existing buildings or to propose guidelines for new constructions against the impact of PDCs, our map of Figure 7a suggests that already a few km away from the volcano, but still well inside the red zone, actions for protecting openings and walls (which are the weaker elements of buildings) against a dynamic pressure of a few kPa could be economically viable.

Concerning the effects of PDCs on the population caught unprotected over free space, the combination of data from maps of particle volumetric concentration, temperature and flow duration of Figure 7 b, c, and d, respectively, allows to assess that even in distal zones, where the mechanical effect of dynamic pressure drastically decays, the effect of hot fine-ash needs to be considered as a primary impact over the population. In fact, it is emerging that even in areas far from a volcano, where particle

https://doi.org/10.5194/egusphere-2024-2971
Preprint. Discussion started: 9 October 2024

concentration, temperature and dynamic pressure strongly decrease, people engulfed in the flow have "high probability of receiving fatal skin burns and inhalation injury of the upper and lower respiratory tract, unless the duration is very brief" (Baxter et al., 2017). The presence of fine-ash particles suspended in air for a long time, even in very small amounts, can be very harmful to human health, and represents one major cause of injury (Horwell and Baxter, 2006). Our maps show that temperature decays from 500°C in the zone characterized by the massive undercurrents around the cone, which is justified by the high particle volumetric concentration, down to values lower than 200°C at the margin of the red zone (Figure 7b). This decrease is due to the large volume of cold air entrained in the current during runout. The low temperature of the PDCs of the 79 AD eruption calculated at Pompeii (about 115°C) is due to the much higher content of cold atmosphere air in the current, with respect to the hot magmatic gas. Exposure to pure hot air at 200–250 °C can be survived for 2–5 minutes (Buettner, 1950), but the presence of inhalable hot fine ash drastically reduces survival times (Baxter et al., 2017). As expected, our map of particle concentration (Figure 7c) shows an abrupt decay passing from the area around the cone, which is characterized by the massive undercurrent, to values much lower than 0.001, typical of the dilute overlying current in distal reaches. Even a volumetric concentration of ash in suspension this low can be unbreathable and is one of the main causes of mortality of PDCs. This is consistent with the observation of historical eruptions, where the flow lasted for several minutes to hours (Lube et al., 2007). During that period the territory was engulfed by thick, expanded, fast and hazardous currents, loaded with unbreathable hot ash (Horwell and Baxter, 2006).

The exposure time becomes indeed a major factor in determining the impact of PDCs on population, since it quantifies the residence time of hot volcanic ash that can be inhaled by people potentially exposed to the currents (Horwell and Baxter, 2006). Our map of Figure 7d, shows that flow duration ranges always exceeds several minutes. These values refer only to the overlying dilute currents, since the massive undercurrent, that freeze at the foot of the cone are much shorter lived. In the case of Pompei eruption of 79 AD a value of 17 min had been calculated, which combined with the concentration of ash particles (about 0.001), was a long enough time to cause death by asphyxia at Pompeii.

There are reports of recent eruptions showing that in the marginal reaches of the current, where the flow duration was only a few minutes, people were able to survive (Baxter et al., 2017). In other cases, longer flow durations did not permit survival and death was caused by fine-ash inhalation (Baxter et al., 2017; Nakada, 2000). Flow duration is a key factor for assessing the impact of PDCs on human beings, especially in distal areas, where the primary risk to life is asphyxiation, as at Pompeii. We agree with Baxter et al. (2017) that the emergency planning for explosive eruptions should concentrate on the distal parts of PDCs where survival could be likely, and where the primary risk to life is asphyxiation from ash inhalation, rather than thermal or mechanical injury. It is important to take note of such information when projecting for emergency plans and risk-reduction measures.

Now, considering that multiple closely-timed currents characterize the sequence of events of eruptions at Vesuvius, it seems quite unlikely the survival of people caught unprotected even at the margin of the red zone.

https://doi.org/10.5194/egusphere-2024-2971
Preprint. Discussion started: 9 October 2024

5 Conclusion

Among volcanic phenomena, PDCs represent the major cause of destruction and injuries in urbanized areas. Since it is impossible to predict the exact dispersal area or the magnitude of an eruption, a probabilistic approach that accounts for the variability of the intensity of pyroclastic density currents of past eruptions is a better choice to inform structural mitigation and, in case of an impending eruption, sustainable evacuation plans.

Starting from data of deposits of past eruptions, by means of a physical model of the current, the probability density function of impact parameters has been calculated at each deposit location. By considering the 84th percentile of the distribution as a safety value, hazard maps have been drawn that show the distribution over the territory of pyroclastic density currents intensity in the long term. These maps differ from the red-zone map of the Italian Civil Protection Department in two main aspects:

1. Our maps include the distribution of the PDCs intensity (as represented by impact parameters). In contrast, the red-zone map is undifferentiated since it was constructed simply by delineating the outer margin of deposit dispersal, but not the PDCs intensities. In fact, the red-zone map is used to delimit the area to be evacuated, and not to project for possible mitigation actions.
2. Our maps are extended more toward northwest with respect to the red-zone map, because in our case all eruptions of Vesuvius are included, while in the construction of the red-zone map the Avellino and Pompeii eruptions were not considered, because it was assumed that eruptions that big should not occur. Actually, it is not the scale of the entire eruption (in terms of total material emitted) that is proportional to the intensity of a PDC, since one single PDC is a small fraction of the total volume. An example is that the bigger eruption of Pompeii had weaker currents than the smaller eruption of Pollena.

It is indeed to note that since our maps extend a little bit more toward northwest with respect to the red-zone map of the Department of Civil Protection of Italy, it should be useful to consider an extension over that direction of the evacuation zone around Vesuvius.

In this study, an integrated model resolving the impact parameters of both the underlying massive part and of the overlying dilute part of the current was used, allowing to differentiate their respective impact. The Bingham plastic rheology used to approximate the massive underflow is similar to that proposed for other massive flows that occur both on volcanoes and on sedimentary terrains. To our knowledge this is the first time that such an integrated approach, resolving the complexity of both the concentrated and the dilute part of the flow, is used for constructing hazard maps, and deserves to be taken into consideration also on other volcanoes that show a complex stratigraphy of PDCs. Such complex stratigraphy, at Vesuvius, implies that during an explosive eruption multiple currents occur, making it reasonable to assume that PDCs can continue for hours or days or more, and that their multiple, cascading effect, need to be considered when projecting for mitigation actions. The maps of impact parameters make it possible to back calculate the initial and boundary conditions of PDCs at the crater and to simulate, by 3D Computational Fluid Dynamics, the propagation of currents over the actual morphology, including the urbanized area around the Vesuvius, which is the next step of the present research.

https://doi.org/10.5194/egusphere-2024-2971
Preprint. Discussion started: 9 October 2024

Our choice of the 84th percentile as a safety value could appear as a particularly severe one, but it is often used in Geophysics and in Engineering (Bradley, 2011; Fang et al., 2020), so we decided to comply with this value. The PYFLOW code allows, anyway, to reconstruct any percentile of the probability density function of the impact parameters, in case other percentiles should be preferred for the emergency planning.

The precision of parameters used in the PYFLOW code needs to be tested against alternatives to assess the modelling approach's epistemic uncertainty. An extension of this work will be dedicated to such a subject, in order to assess the multimodel variability of results. We think, anyway, that the method used here to prospect probabilistically the hazard in the long term, and to take as a safety value the 84th percentile of PDF, covers an ample range of the aleatoric uncertainty of results, likely covering also the higher end of the epistemic uncertainty.

Appendix A. The flow model and the numerical code

The reconstruction of the impact parameters of PDCs is based on a flow model that starts with the assumption that the current is velocity and density stratified (Valentine, 1987; Dellino et al., 2008; Brown and Branney, 2013). The model is implemented in the Fortran numerical code PYFLOW v2.5 (Dioguardi and Dellino, 2014; Dioguardi and Mele, 2018).

In the stratified multiphase gas-particle current, the basal part is a shear flow that moves attached to the ground and has a density higher than atmosphere. The upper part is buoyant, because particle concentration decreases with height down to a value that, combined with the effect of gas temperature, makes the mixture density lower than the surrounding atmosphere.

The inputs needed, in our model, for the calculation of the impact parameters are reported in the input files of the Zenodo repository (Mele et al. 2024). Some of the input data are obtained directly in the field, such as deposit and layer thickness. Deposit density is obtained by weighing a known volume of deposit. Other data come from laboratory analyses on samples extracted from the deposit. In the laboratory, first, the grain-size distribution is determined, then from each size class a sample of particles per each component (crystal, glass, lithics) is extracted, and density data are obtained on such particle samples by means of pycnometers (Mele et al., 2015). Particle shape parameters, which are needed for the calculation of settling velocity, are obtained by image analysis methods (Mele et al., 2011).

In a dilute PDC, particles are mainly transported by turbulent suspension and sedimentation is controlled by a balance between flow shear velocity u_*, which is controlled by fluid turbulence and favours suspension, and particle settling velocity w_t:

$$w_t = \sqrt{\frac{4gd(\rho_s - \rho_{mix})}{3C_d\rho_{mix}}} \quad \text{(A1)}$$

which favours sedimentation, where g is gravity acceleration, d is particle size, ρ_s is the particle density, ρ_{mix} is the bulk flow density and C_d is drag coefficient. The median of the grain-size distribution was used for particle size. PYFLOW allows selecting among multiple shape-dependent drag laws; in this work, the drag law of Dioguardi et al. (2018) was used. The capacity of a current to transport particles in suspension is quantified by the Rouse number (Rouse, 1939) $P_n = \frac{w_t}{ku_*}$, where k

https://doi.org/10.5194/egusphere-2024-2971
Preprint. Discussion started: 9 October 2024

is the Von Karman constant (0.4). At the limit of transportation by turbulent suspension when $P_n = 2.5$, from its defitinion, since k=0.4, it follows that:

$$w_t = u_* \quad \text{(A2)}$$

This is the suspension-sedimentation criterion (Middleton and Southard, 1984), which means that particles stay suspended until their settling velocity is less than the flow shear velocity. In other terms, particles in the deposit that are settled from suspension (the laminae-forming bed load) give an indication of the current shear velocity, once their terminal velocity is defined. Upon combining (A1) and (A2), it follows that:

$$u_*^2 = \frac{4gd(\rho_s - \rho_{mix})}{3C_d\rho_{mix}} \quad \text{(A3)}$$

which leads to the shear stress at the base of the current:

$$\tau = \rho_{mix}u_*^2 \quad \text{(A4)}$$

There can be also particles that are never transported in suspension but can be moved over the substrate by the overlying current's shear stress (e.g., particles for which $P_n > 2.5$ or that are already on the ground before the passage of the dilute PDC). The latter phenomenon can be described by the Shield or entrainment criterion (Miller et al., 1977), which compares the dilute PDC shear stress to the buoyancy force of the coarse particle in the flow:

$$\theta = \frac{\rho_{mix}u_*^2}{(\rho_{s,ent} - \rho_{mix})gd_{ent}} \quad \text{(A5)}$$

where $\rho_{s,ent}$ and d_{ent} are the density and diameter of the entrained particle, respectively; θ is a parameter which is equal to 0.015 for a particle Reynolds number $Re_* = \frac{\rho_{mix}u_*d_{ent}}{\mu}$ (where μ is the fluid viscosity) larger than 1000 (Miller et al., 1977), a condition that holds for most dilute PDCs (Dellino et al. 2008).

Both methods are implemented in PYFLOW v2.5 and can be alternatively activated depending on the PDC's deposit's architecture. When the typical complete stratigraphic sequence attributed to a dilute DPDC is observed (e.g., Figure 1c), that is:

1. a coarse layer of lapilli and bombs moved by shear at the base of the current;
2. a laminated layer of ash formed by particles settled from turbulent suspension)

it is possible to apply both the Shield and the suspension-sedimentation criteria for calculating the flow parameters. However, the layer of entrained coarse lapilli or bombs, which is typical of proximal locations around the eruptive vent, is often missing in distal outcrops, thus preventing to use the Shield criterion far away from the volcanic vent. In that case, an alternative method based on the hydraulic equivalence of particles can be used.

In both cases the parameters needed to calculate the vertical profiles of velocity, particle concentration (hence flow density), flow temperature and dynamic pressure are obtained. Specifically, the velocity profile $u(z)$ follows the equation of a turbulent boundary layer shear flow moving over a rough surface (Furbish, 1997):

$$\frac{u(z)}{u_*} = \frac{1}{k}\ln\frac{z}{k_s} + 8.5 \quad \text{(A6)}$$

where k_s is the roughness parameter of the substrate. The concentration profiles is taken from Rouse (1939):

https://doi.org/10.5194/egusphere-2024-2971
Preprint. Discussion started: 9 October 2024

$$C(z) = C_0 \left(\frac{z_0}{z_{tot}-z_0}\frac{z_{tot}-z}{z}\right)^{Pn} \quad \text{(A7)}$$

in which z_{tot} is the total flow thickness, z_0 is the height at which the particle concentration is known (C_0). From (A7), the flow bulk density profile can be defined as:

$$\rho_{mix}(z) = \big(1 - C(z)\big)\rho_g + C(z)\rho_s \quad \text{(A8)}$$

PYFLOW first estimates the shear flow height z_{sf} by solving the system of equations composed of eq. (A4) and:

$$\tau = (\rho_{mix} - \rho_{atm}) g \sin\alpha \, z_{sf} \quad \text{(A9)}$$

where ρ_{atm} is the atmospheric density and α is the slope of the ground, measured in the field, on which the dilute PDC was flowing.

The shear current is composed of gas and a mixture of particles, in which those with $P_n = 2.5$ are at settling condition. Finer particles are held in suspension by turbulent stress and contribute to the concentration profile $C(z)$, but their average Rouse number $P_{n,susp}$, which is lower than 2.5, is unknown. In addition, the thickness of the PDC z_{tot} and the flow gas density ρ_g are unknown. In order to get these three unknowns, PYFLOW solves for the following system of three equations:

$$\rho_{atm} = \rho_g + \left((\rho_s - \rho_g) C_0 \left(\frac{z_0}{z_{tot}-z_0}\frac{z_{tot}-z_{sf}}{z_{sf}}\right)^{Pn,susp} \right) \quad \text{(A10)}$$

$$\rho_{mix} = \frac{1}{z_{sf}-z_0}\int_{z_0}^{z_{sf}} \left[\rho_g + \left((\rho_s - \rho_g) C_0 \left(\frac{z_0}{z_{tot}-z_0}\frac{z_{tot}-z}{z}\right)^{Pn,susp} \right) \right] dz \quad \text{(A11)}$$

$$z_{tot} = \frac{H_{lam}}{C} = \frac{z_{lam}}{\frac{\rho_{mix}-\rho_g}{\rho_s-\rho_g}} \quad \text{(A12)}$$

The first equation (A10) states that the atmospheric density is reached at the top of the shear flow z_{sf}; the second one (A11) defines the average flow density calculated between z_0 and z_{sf}; the third equation (A12) defines the total flow thickness as the ratio between the thickness of the laminated layer H_{lam} in the deposit and the average concentration in the flow C, which is defined as:

$$C = \frac{\rho_{mix}-\rho_g}{\rho_s-\rho_g} \quad \text{(A13)}$$

In this work C_0 is set to the maximum packing for pyroclastic particles (0.7) (Dellino et al., 2008), hence z_0 is taken as the minimal sedimenting thickness.

Subsequently, PYFLOW uses ρ_g to calculate the flow temperature profile $T(z)$, assuming the flow is composed by the solid particles, the magmatic gas and entrained air, if the user provides in input: the temperature of the magmatic gas T_m, the air temperature T_a (set by default to 293 K if not provided), the temperature of the solid particles T_s, the specific gas constant of the magmatic gas R_m and air R_a (set by default to 287 J kg^{-1} K^{-1}), the specific heat at constant pressure of the magmatic gas Cp_m and of the solid particles Cp_s and the average density of the solid particles ρ_s. First, the density of the magmatic gas and entrained air are obtained by solving for the equation of state:

$$\rho_m = \frac{p_a}{R_a T_a} \quad \text{(A14a)}$$

https://doi.org/10.5194/egusphere-2024-2971
Preprint. Discussion started: 9 October 2024

$$\rho_a = \frac{p_a}{R_m T_m} \quad \text{(A14b)}$$

hence with the assumption that the gas phases are at constant atmospheric pressure (set to 101325 Pa if not specified in input by the user). From these densities and the flow gas density ρ_g, one can calculate the relative volumetric concentration of the magmatic gas $C_{gm,rel}$ and entrained air $C_{gm,rel}$:

$$C_{gm,rel} = \frac{\rho_g - \rho_a}{\rho_m - \rho_a} \quad \text{(A15a)}$$

$$C_{ga,rel} = 1 - C_{gm} \quad \text{(A15b)}$$

These concentrations are still not the real magmatic gas $C_{g,m}$ and entrained air $C_{g,a}$ volumetric concentrations in the multiphase flow that includes the solid particle concentration calculated C via Eq. (A13), hence they need to be rescaled so that the sum of their rescaled values equals 1-C:

$$C_{g,m} = C_{gm,rel}(1 - C) \quad \text{(A16a)}$$

$$C_{g,a} = C_{ga,rel}(1 - C) \quad \text{(A16b)}$$

Finally, the flow temperature can be calculated using the following equation:

$$T(z) = \frac{\rho_m C_{g,m}(z) T_m Cp_m + \rho_a C_{g,a}(z) T_a Cp_a + \rho_s C(z) T_s Cp_s}{\rho_m C_{g,m}(z) Cp_m + \rho_a C_{g,a}(z) Cp_a + \rho_s C(z) Cp_s} \quad \text{(A17)}$$

By combining the velocity (A6) and density (A8) profiles, the dynamic pressure profile is finally obtained:

$$P_{dyn}(z) = \frac{1}{2}\rho_{mix}(z) u(z)^2 \quad \text{(A18)}$$

Concerning flow duration, in a PDC, sedimentation occurs at a rate S_r that represents the mass of particles settling over a unit area in the unit time. Deposit thickness grows by aggradation of particles during the time-integrated passage of the current. The aggradation rate A_r, which is the rate at which deposit thickness grows, is equal to the sedimentation rate divided by deposit density ρ_{dep}. The total time of aggradation, t, which is a proxy of flow duration, is equal to deposit thickness H_{dep} divided by A_r:

$$t = \frac{H_{dep}}{A_r} \quad \text{(A19)}$$

Deposit density and thickness are measured in the field, consequently the only missing quantity for the calculation of flow duration is the sedimentation rate.

Dellino et al. (2019), recently proposed a model for the calculation of the sedimentation rate:

$$S_r = \left(\sum_i^n \rho_{s_i} w_{t_i} \left(\frac{\frac{\phi_i / \rho_{s_i}}{\sum_{i=1}^n \phi_i / \rho_{s_i}} * C_{tot}}{\left(\left(10.065 * \frac{P_{ni}}{P_n^*} \right) + 0.1579 \right)} * 0.7 + \frac{\frac{\phi_{i+1} / \rho_{s_i+1}}{\sum_{i=1}^n \phi_{i+1} / \rho_{s_{i+1}}} * C_{tot}}{\left(\left(10.065 * \frac{P_{ni}}{P_n^*} \right) + 0.1579 \right)} * 0.3 \right) \right) - 0.01 \quad \text{(A20)}$$

with the subscript i referring to the ith particle-size class, n being the number of size classes of the grain-size distribution of the sediment, ϕ_i, ρ_{si} and P_{ni} being the weight fraction, the density and the Rouse number of the ith grain-size fraction, respectively.

https://doi.org/10.5194/egusphere-2024-2971
Preprint. Discussion started: 9 October 2024

$P_n^* = \frac{P_{n,avg}}{P_{n.susp}}$ is the normalized Rouse number of the current, i.e., the ratio between the average Rouse number of the solid material in the current and the Rouse number at maximum suspension capacity. The model considers the contribution of each size class of particles to the sedimentation, and not the average grain size, because the solid load constituting a suspension current, especially in the case of PDCs, is made up of a mixture of different components (lithics, glassy fragments and crystals) with different size, density and shape, thus different terminal velocity. The average Rouse number of the solid material in the current is calculated as the average of the particulate mixture:

$$P_{n_{avg}} = \sum_{i=1}^{n} P_{ni}\, C_i / C \quad \text{(A21)}$$

When $P_n^* > 1$, a current has a particle volumetric concentration in excess of its maximum capacity, e.g. it is over-saturated of particles, which favours sedimentation. When it is lower than 1, a current has a particle volumetric concentration lower than its maximum capacity, e.g. it is under-saturated, and could potentially include additional sediment in suspension by erosion from the substrate. For more details see Dellino et al. (2019).

Finally, PYFLOW calculates probability density functions of all the parameters presented above starting from a Gaussian distribution. From these functions, it is possible to obtain the values of the impact parameters at the desired exceedance probability.

Code availability

PYFLOW v2.5 is available at https://github.com/FabioDioguardi/PYFLOW/releases/tag/v_2.5.

Data availability

All supporting data, which include input and output files of the DPDCs simulations carried out with PYFLOW, calculations of the massive PDCs' impact parameters and rasterized impact parameters map data are available at https://doi.org/10.5281/zenodo.13378963.

Author contribution

PD developed the methodology and the models and contributed to data analysis and text editing. FD developed PYFLOW v2.5, contributed to the simulations, data analysis and text editing. DM run the simulations with PYFLOW, conducted data analysis and produced the graphical outputs and contributed to text editing. RS contributed to data analysis and text editing.

Competing interests

The authors declare that they have no conflict of interest.

https://doi.org/10.5194/egusphere-2024-2971
Preprint. Discussion started: 9 October 2024

Acknowledgements

This study was carried out within the RETURN Extended Partnership and received funding from the European Union Next-GenerationEU (National Recovery and Resilience Plan – NRRP, Mission 4, Component 2, Investment 1.3 – D.D. 1243 2/8/2022, PE0000005).

References

Baxter, P. T., Neri, A., and Todesco, M.: Physical modeling and human survival in pyroclastic flows, Nat. Hazards, 17, 163-176, 1998.

Baxter, P.J., Jenkins, S., Rosadi, S., Komorowski, J. C., Dunn, K., Purser, D., Voight, B., and Shelley, I.: Human survival in volcanic eruptions: thermal injuries in pyroclastic surges, their causes, prognosis and emergency management, Burns 43, 1051-1069, 2017.

Bertagnini, A., Landi, P., Rosi, M., and Vigliargio, A.: The Pomici di Base plinian eruption of Somma-Vesuvius, J. Volcanol. Geotherm. Res., 83, 219–239, 1998.

Bradley, B. A.: Design seismic demands from seismic response analyses: a probability-based approach, Earthq. Spectra 27(1), 213–224, 2011, https://doi.org/10.1193/1.3533035.

Branney, M. J., and Kokelaar, P.: Pyroclastic Density Currents and the Sedimentation of Ignimbrites, Geological Society, London, Memoirs, 27 pp, 2002.

Breard, E.C.P., and Lube, G.: Inside pyroclastic density currents – uncovering the enigmatic flow structure and transport behaviour in large-scale experiments, Earth Planet. Sci. Lett., 458, 22–36, 2017.

Brocchini, D., Principe, C., Castradori, D., Laurenzi, M.A., and Gorla, L.: Quaternary evolution of the southern sector of the Campanian Plain and early Somma-Vesuvius activity: insights from the Trecase 1 well, Mineral. Petrol. 73, 67–91, https://doi.org/10.1007/s007100170011, 2001.

Brown, R. J., and Branney, M. J.: Internal flow variations and diachronous sedimentation within extensive, sustained, density stratified pyroclastic density currents down gentle slopes, as revealed by the internal architectures of ignimbrites in Tenerife. Bull. Volcanol., 75, 1–24, 2013.

Buettner, K.: Effects of extreme heat in man, J. Am. Med. Assoc. 144, 732–738, 1950.

Cao, Z., Egashira, S., and Carling, P. A.: Role of suspended-sediment particle size in modifying velocity profiles in open channel flows, Water Resour. Res., 39(2), 1029, doi:10.1029/2001WR000934, 2003.

Capra, L., Sulpizio, R., Marquez-Ramirez, V.H., Coviello, V., Doronzo, D.M., Arambula-Mendoza, R., and Cruz, S.: The anatomy of a pyroclastic density current: the 10 July 2015 event at Volc an de Colima (Mexico), Bull. Volcanol., 80, 34, 2018.

Cioni, R., Marianelli, P., and Sbrana, A.: Dynamics of the AD 79 eruption: stratigraphic, sedimentological and geochemical data on the succession from the Somma-Vesuvius southern and eastern sectors, Acta Volcanol. 2,109–123, 1992.

https://doi.org/10.5194/egusphere-2024-2971
Preprint. Discussion started: 9 October 2024

Cioni, R., Santacroce, R., and Sbrana, A.: Pyroclastic deposits as a guide for reconstructing the multi-stage evolution of the Somma-Vesuvius caldera, Bull. Volcanol., 60, 207–222, 1999.

Cioni, R., Sulpizio, R., and Garruccio, N.: Variability of the eruption dynamics during a subplinian event: the Greenish Pumice eruption of Somma-Vesuvius (Italy), J. Volcanol. Geotherm. Res., 124, 89–114, 2003.

Cioni, R., Gurioli, L., Lanza, R., and Zanella, E.: Temperatures of the A. D. 79 pyroclastic density current deposits (Vesuvius, Italy), J. Geophys. Res., 109, B02207, 2004.

Cioni, R., Bertagnini, A., Santacroce, R., and Andronico, D.: Explosive activity and eruption scenarios at Somma-Vesuvius (Italy): towards a new classification scheme, J. Volcanol. Geotherm. Res. 178:331–346, doi:10.1016/j.jvolgeores.2008.04.024, 2008.

Civil Protection Department, Presidency of the Council of Ministers, Italian Government: Direttiva del 14 febbraio 2014: disposizioni per l'aggiornamento della pianificazione di emergenza per il rischio vulcanico del Vesuvio, Gazzetta Ufficiale, 108, https://www.protezionecivile.gov.it/en/normativa/direttiva-del-14-febbraio-2014/, 2014.

Cole, P. D., and Scarpati, C.: The 1944 eruption of Vesuvius, Italy: Combining contemporary accounts and field studies for a new volcanological reconstruction, Geol. Mag., 147, 391-415, 2010.

Crook, C., and Rouberyrie, L.: QGIS Countour plugin, https://github.com/ccrook/QGIS-Contour-Plugin, 2024.

Dellino, P., Mele, D., Sulpizio, R., La Volpe, L., and Braia, G.: A method for the calculation of the impact parameters of dilute pyroclastic density currents based on deposit particle characteristics, J. Geophys. Res., 113, B07206, https://doi.org/10.1029/2007B005365, 2008.

Dellino, P., Büttner, R., Dioguardi, F., Doronzo, D. M., La Volpe, L., Mele, D., Sonder, I., Sulpizio, R., and Zimanowski, B.: Experimental evidence links volcanic particle characteristics to pyroclastic flow hazard, Earth Planet. Sci. Lett., 295, 314–320, 2010.

Dellino F., Dioguardi F., Doronzo D.M., and Mele D.: The entrainment rate of non Boussinesq hazardous geophysical gas-particle flows: an experimental model with application to pyroclstic density currents, Geophys. Res. Lett., 46 (22), 12851-12861, 2019.

Dellino, P., Dioguardi, F., Doronzo, D. M., and Mele, D.: A discriminatory diagram of massive versus stratified deposits based on the sedimentation and bedload transportation rates. Experimental investigation and application to pyroclastic density currents, Sedimentology 67, 2013–2039, doi:10.1111/sed.12693, 2020.

Dellino, P., Dioguardi, F., Isaia, R., Sulpizio, R., and Mele, D:. The impact of pyroclastic density currents duration on humans: the case of the AD 79 eruption of Vesuvius. Sci. Rep. 11, 4959, 2021.

Dioguardi, F., and Dellino, P.: PYFLOW: a computer code for the calculation of the impact parameters of dilute pyroclastic density currents (DPDC) based on field data, Comput. Geosci., 66, 200–210, doi:1 0.1016/j.cageo.2014.01.013, 2014.

Dioguardi, F., and Mele, D.: PYFLOW_2.0: a computer program for calculating flow properties and impact parameters of past dilute pyroclastic density currents based on field data, Bull. Volcanol. 80, 28, 2018.

https://doi.org/10.5194/egusphere-2024-2971
Preprint. Discussion started: 9 October 2024

Dioguardi, F., Mele, D., and Dellino, P.: A New One-Equation Model of Fluid Drag for Irregularly Shaped Particles Valid Over a Wide Range of Reynolds Number, J. Geophys. Res. Solid Earth 123(1), 144-156, https://doi.org/10.1002/2017JB014926, 2018.

Druitt, T. H.: Emplacement of the 18 May 1980 lateral blast deposit ENE of Mount St. Helens, Washington, Bull. Volcanol., 54, 554–572, 1992.

Druitt, T. H., and Kokelaar P.: The Eruption of Soufrie´re Hills Volcano, Montserrat, From 1995 to 1999, Geol. Soc. Lond. Mem., 21, 664, 2002.

Esposti Ongaro, T., Neri, A., Menconi, G., de'Michieli Vitturi, M., Marianelli, P., Cavazzoni, C., Erbacci, G., and Baxter, P.J.: Transient 3Dnumerical simulations of column collapse and pyroclastic density current scenarios at Vesuvius, J. Volcanol. Geotherm. Res., 178, 378–396, 2008.

Fang. C., Ping, Y., and Chen, Y.: Loading protocols for experimental seismic qualification of members in conventional and emerging steel frames, Earthquake Engng. Struct. Dyn., 49, 155–174, 2020, https://doi.org/10.1002/eqe.3231.

Fink, J. H., Malin, M. C., D'Alli, R. E., and Greeley, R.: Rheological properties of mudflows associated with the spring 1980 eruptions of Mount St. Helens Volcano Washington, Geophys. Res. Lett., 8, 43–46, 1981.

Fisher, R. V.: Transport and deposition of a pyroclastic surge across an area of high relief: the 18 May 1980 eruption of Mount St. Helens, Washington, Geol. Soc. Am. Bull., 102, 1038–1054, 1990.

Furbish, D. J.: Fluid Physics in Geology, 476 pp., Oxford Univ. Press, New York, 1997.

Gernon, T. M., Upton, B. G. J., and Hincks, T. K.: Eruptive history of an alkali basaltic diatreme from Elie Ness, Fife, Scotland, Bull. Volcanol., 75, 704, 2013.

Giordano, G., Zanella, E., Trolese, M., Baffioni, C., Vona, A., Caricchi, C., De Benedetti, A.A., Corrado, S., Romano, C., Sulpizio, R., Geshi, N.: Thermal interactions of the AD79 Vesuvius pyroclastic density currents and their deposits at Villa dei Papiri (Herculaneum archaeological site, Italy), Earth Plan. Sci. Lett., 490, 180-192, https://doi.org/10.1016/j.epsl.2018.03.023, 2018.

Gurioli, L., Zanella, E., Pareschi, M. T., and Lanza, R.: Influences of urban fabric on pyroclastic density currents at Pompeii (Italy): Flow direction and deposition, J. Geophys. Res., 112, B05213, 2007.

Gurioli, L., Sulpizio, R., Cioni, R., Sbrana, A., Santacroce, R., Luperini, W., and Andronico D.: Pyroclastic flow hazard assessment at Somma-Vesuvius based on the geological record, Bull. Volcanol., 72, 1021-1038, 2010.

Horwell, C. J., and Baxter P.: The respiratory health hazards of volcanic ash: A review for volcanic risk mitigation. Bull. Volcanol., 69, 1-24, 2006.

ISTAT: Basi territoriali e variabili censuarie: censimento 2011. 15-Campania. http://www.istat.it/it/files/2013/11/R15_11_WGS84.zip, 2011.

Jenkins, S., Komorowski, J. -C., Baxter, P. J., Spence, R., Picquout, A., Surono, F. L.: The Merapi 2010 eruption: an interdisciplinary assessment methodology for studying pyroclastic density currents, J. Volcanol. Geotherm. Res., 261, 316–329, 2013.

https://doi.org/10.5194/egusphere-2024-2971
Preprint. Discussion started: 9 October 2024

Jones, T.J., Beckett, F., Bernard, B., Breard, E.C.P., Dioguardi, F., Dufek, J., Engwell, S., and Eychenne, J.: Physical properties of pyroclastic density currents: relevance, challenges and future directions, Front. Earth Sci., 11, https://doi.org/10.3389/feart.2023.1218645, 2023.

Kneller, B. C., and Branney, M. J.: Sustained high density turbidity currents and the deposition of thick massive sands, Sedimentology, 42, 607–616, 1995.

Lowe, D. R.: Sedimentary gravity flows: II. Depositional models with special reference to the deposits of high density turbidity currents. J. Sed. Petrol., 52, 279–297, 1982.

Lowe, D. R.: Suspended-load fallout rate an independent variable in the analysis of current structures, Sedimentology, 35, 765–776, 1988.

Lube, G., Cronin, S. J., Platz, T., Freundt, A., Procter, J. N., Henderson, C., and Sheridan, M. F.: Flow and deposition of pyroclastic granular flows: a type example from the 1975 Ngauruhoe eruption, New Zealand, J. Volcanol. Geotherm. Res. 161, 165–186, 2007.

Luongo, G., Perrotta, A., Scarpati, C., De Carolis, E., Patricelli, G., and Ciarallo, A.: Impact of the AD 79 eruption on Pompeii, II. Causes of death of the inhabitants inferred by stratigraphic analysis and areal distribution of the human causalities, J. Volcanol. Geotherm. Res., 126, 169–200, 2003.

Major, J. J., and Pierson, T.C.: Debris flow rheology: experimental analysis of fine-grained slurries, Water Resour. Res., 28, 841–857, 1992.

Major, J. J., and Iverson, R. M.: Debris-flow deposition effects of pore-fluid pressure and friction concentrated at flow margins, Geol. Soc. Am. Bull., 111, 1424–1434, 1999.

Mele, D., Sulpizio, R., Dellino, P., and La Volpe, L.: Stratigraphy and eruptive dynamics of a pulsating Plinian eruption of Somma-Vesuvius: the Pomici di Mercato (8900 years B.P.), Bull. Volcanol. 73, 257–278, 2011.

Mele, D., Dioguardi, F., Dellino, P., Isaia, R., Sulpizio, R., and Braia, G.: Hazard of pyroclastic density currents at the Campi Flegrei Caldera (Southern Italy) as deduced from the combined use of facies architecture, physical modeling and statistics of the impact parameters, J. Volcanol. Geoth. Res., 299, 35–53, 2015.

Mele, D., Dellino, P., Dioguardi F.: Pyroclastic density currents hazard simulation data at Mt. Vesuvius, Italy [Data set], Zenodo, https://doi.org/10.5281/zenodo.13682628, 2024.

Middleton, G. V., and Southard, J. B.: Mechanics of Sediment Movement, 401 pp., Soc. Econ. Paleont. Miner., Tulsa, 1984.

Miller, M.C., McCave, I.N., and Komar, P.D.: Threshold of sediment motion under unidirectional currents. Sedimentology, 24, 507–527, 1977.

Nakada, S.: Hazards from Pyroclastic Flows and Surges, In Encyclopedia of Volcanoes (eds Sigurdsson, H. et al.), Academic Press, Cambridge, 2000.

Neri, A., Esposti Ongaro, T., Menconi, G., Vitturi, M., De'Michieli, M., Cavazzoni, C., Erbacci, G., and Baxter, P.J.: 4D simulation of explosive eruption dynamics at Vesuvius, Geophys. Res. Lett., 34(4), L04309, 2007.

https://doi.org/10.5194/egusphere-2024-2971
Preprint. Discussion started: 9 October 2024

Palladino, D.M., and Valentine, G.A.: Coarse-tail vertical and lateral grading in pyroclastic flow deposits of the Latera Volcanic Complex (Vulsini, Central Italy): origin and implications for flow dynamics, J. Volcanol. Geoth. Res., 69, 343–364, 1995.

Postma, G., Cartigny, M., and Kleverlaan, K.: Structureless, coarse-tail graded Bouma Ta formed by internal hydraulic jump of the turbidity current, Sed. Geol., 219, 1–6, 2009.

QGIS.org: QGIS Geographic Information System. Open Source Geospatial Foundation Project, http://qgis.org, 2024.

Rosi, M., Principe, C., Vecci, R.: The 1631 eruption of Vesuvius reconstructed from the review of chronicles and study of deposits, J. Volcanol. Geotherm. Res., 58, 151–182, 1993.

Rouse, H.: An analysis of sediment transportation in the light of fluid turbulence, in Soil Conservation Services Report No. SCS-TP-25, USDA, Washington, D.C., 1939.

Santacroce, R., Cioni, R., Marianelli, P., Sbrana, A., Sulpizio, R., Zanchetta, G., Don-ahue, D. J., and Joron, J.-L.: Age and whole rock-glass composition of proximal pyroclastics from the major explosive eruptions of Somma–Vesuvius: a review as a tool for distal tephrostratigraphy, J. Volcanol. Geotherm. Res.177, 1–18, 2008.

Selva, J., Sandri, L., Taroni, M., Sulpizio, R., Tierz, P., and Costa, A: A simple two-state model interprets temporal modulations in eruptive activity and enhances multivolcano hazard quantification, Sci. Adv., 8(44), eabq4415, https://doi.org/10.1126/sciadv.abq4415, 2022.

Sevink, J., van Bergen, M. J., van der Plicht, J., Feiken, H., Anastasia, C., and Huizinga, A.: Robust date from the Bronze Age Avellino eruption (Somma–Vesuvius): 3945 ±10calBP(1995± 10 cal BC), Quat. Sci. Rev.30, 1035–1046, 2011.

Sigurdsson, H., Carey, S., Cornell, W., and Pescatore, T.: The eruption of Vesuvius in 79 AD, Nat. Geogr. Res., 1, 332–387, 1985.

Spence, R. J. S., Baxter, P. J., and Zuccaro G.: Building vulnerability and human casualty estimation for a pyroclastic flow: A model and its application to Vesuvius, J. Volcanol. Geotherm. Res., 133, 321– 343, 2004.

Sulpizio, R., Mele, D., Dellino, P., and LaVolpe, L.: A complex, Subplinian type eruption from low-viscosity, tephri-phonolitic magma: the Pollena eruption of Somma-Vesuvius (Italy), Bull. Volcanol. 67(8), 743–767, https://doi.org/10.1007/s00445-005-0414-x, 2005.

Sulpizio, R., Mele, D., Dellino, P., and La Volpe, L.: Deposits and physical properties of pyroclastic density currents during complex Subplinian eruptions: The AD 472 (Pollena) eruption of Somma-Vesuvius, Italy, Sedimentology, doi:10.1111/j.1365-3091.2006.00852.x, 2007.

Sulpizio, R., Bonasia, R., Dellino, P.,Mele, D., Di Vito,M.A., amd La Volpe, L.: The Pomici di Avellino eruption of Somma-Vesuvius (3.9 ka BP). Part II: Sedimentology and physical volcanology of pyroclastic density current deposits, Bull. Volcanol., 72, 559–577, 2010a.

Sulpizio, R., Cioni, R., Di Vito, M.A., Mele, D., Bonasia, R., and Dellino, P.: The Pomici di Avellino eruption of Somma–Vesuvius (3.9 ka BP) part I: stratigraphy, compositional variability and eruptive dynamics, Bull. Volcanol. 72, 539-558, 2010b.

https://doi.org/10.5194/egusphere-2024-2971
Preprint. Discussion started: 9 October 2024

Sulpizio, R., Dellino, P., Doronzo, D. M., and Sarocchi, D.: Pyroclastic density currents: state of the art and perspectives, J. Volcanol. Geoth. Res., 283, 36–65, 2014.

Sulpizio, R., Castioni, D., Rodriguez-Sedano, L. A., Sarocchi, D., and Lucchi, F.: The influence of slope-angle ratio on the dynamics of granular flows: insights from laboratory experiments, Bull. Volcanol., 78(11), 1–11, 2016.

Talling, P. J., Amy, L. A., Wynn, R. B., Peakall, J., and Robinson, M.: Beds comprising debrite sandwiched within co-genetic turbidite: origin and widespread occurrence in distal depositional environments, Sedimentology, 51, 163–194, 2004.

Tarquini, S., Isola, I., Favalli, M., Battistini, A., and Dotta, G.: TINITALY, a digital elevation model of Italy with a 10 meters cell size (Version 1.1). Istituto Nazionale di Geofisica e Vulcanologia (INGV). https://doi.org/10.13127/tinitaly/1.1, 2023.

Valentine, G. A.: Stratified flow in pyroclastic surges, Bull. Volcanol. 49, 616–630, 1987.

Valentine, G. A.: Damage to structures by pyroclastic flows and surges, inferred from nuclear weapons effects, J. Volcanol. Geotherm. Res., 49, 616– 630, 1998.

Woods, A. W., Sparks, R. S. J., Ritchie, L. J., Batey, J., Gladstone, C., and Bursik, M. I.: The explosive decompression of a pressurized volcanic dome: the 26 December 1997 collapse and explosion of Soufrière Hills Volcano, Montserrat, Geol. Soc. London Mem., 21, 457-465, 2002.

Zanchetta, G., Sulpizio, R., Pareschi, M.T., Leoni, F.M., and Santacroce, R.: Characteristics of May 5–6 1998 volcaniclastic debris flows in the Sarno area (Campania, Southern Italy): relationships to structural damage and hazard zonation, J. Volcanol. Geotherm. Res. 133:377–393, 2004.

Zuccaro, G., Cacace, F., Spence, R. J. S., and Baxter, P. J.: Impact of explosive eruption scenarios at Vesuvius, J. Volcanol. Geotherm. Res., 178, 416-453, 2008.

Zuccaro, G., and Leone, M.: Building Technologies for the Mitigation of Volcanic Risk: Vesuvius and Campi Flegrei, Nat. Hadards Rev., 13, 221-232, 2012.